Differential splicing and glycosylation of Apoer2 alters synaptic plasticity and fear learning

Catherine R. Wasser[1,2,*,>†], **Irene Masiulis**[2,†], **Murat S. Durakoglugil**[1,2], **Courtney Lane-Donovan**[1,2], **Xunde Xian**[1,2], **Uwe Beffert**[2], **Anandita Agarwala**[2], **Robert E. Hammer**[3], and **Joachim Herz**[1,2,4,5,*]

[1]Center for Translational Neurodegeneration Research, University of Texas Southwestern Medical Center, Dallas, TX 75390, USA

[2]Department of Molecular Genetics, University of Texas Southwestern Medical Center, Dallas, TX 75390–9046, USA

[3]Department of Biochemistry, University of Texas Southwestern Medical Center, Dallas, TX 75390, USA

[4]Department of Neurology and Neurotherapeutics, University of Texas Southwestern Medical Center, Dallas, TX 75390, USA

[5]Department of Neuroscience, University of Texas Southwestern Medical Center, Dallas, TX 75390, USA

Abstract

Apoer2 is an essential receptor in the central nervous system that binds to the apolipoprotein ApoE. Various splice variants of Apoer2 are produced. We showed that *Apoer2* lacking exon 16, which encodes the O-linked sugar (OLS) domain, altered the proteolytic processing and abundance of *Apoer2* in cells and synapse number and function in mice. In cultured cells expressing this splice variant, extracellular cleavage of OLS-deficient Apoer2 was reduced, consequently preventing γ-secretase-dependent release of the intracellular domain of Apoer2. Mice expressing Apoer2 lacking the OLS domain had increased Apoer2 abundance in the brain, hippocampal spine density, and glutamate receptor abundance, but decreased synaptic efficacy. Mice expressing a form of Apoer2 lacking the OLS domain and containing an alternatively spliced cytoplasmic tail region that promotes glutamate receptor signaling showed enhanced hippocampal long-term potentiation (LTP), a phenomenon associated with learning and memory. However, these mice did not display enhanced spatial learning in the Morris water maze, and cued fear conditioning was reduced. Reducing the expression of the mutant *Apoer2* allele so that the

---

abundance of the protein was similar to that of Apoer2 in wild-type mice normalized spine density, hippocampal LTP, and cued fear learning. These findings demonstrated a role for ApoE receptors as regulators of synaptic glutamate receptor activity and established differential receptor glycosylation as a potential regulator of synaptic function and memory.

Introduction

Alzheimer's disease is a progressive neurodegenerative illness marked by accumulation of amyloid plaques and neurofibrillary tangles. Amyloid plaques are aggregates of amyloid-β (1, 2), a product of amyloid precursor protein (APP) cleavage (3). Perfusion of otherwise healthy brain slices with oligomeric amyloid-β decreases long-term potentiation (LTP) and enhances long-term depression (LTD), which suggests that the synaptic dysfunction found early in Alzheimer's disease is likely amyloid-β–driven (4–6). We have shown previously that neuronal apolipoprotein E (ApoE) receptor signaling counteracts the synaptic suppression induced by amyloid-β (4, 7); ApoE4 genotype is the most prevalent risk factor for late-onset Alzheimer's disease(8, 9); and ApoE4, which differs by a single amino acid from the more frequent ApoE3 form, selectively impairs the protective effect of Reelin by sequestering the ApoE receptor Apoer2, together with α -amino-3-hydroxy-5-methyl-4-isoxazolepropionic acid (AMPA)– and N-methyl-D-aspartate (NMDA)– type glutamate receptors, in the recycling endosome(10). These results implicate Apoer2 in the synaptic dysfunction that is one of the earliest manifestations of Alzheimer's disease, whereby ApoE4 impairs Apoer2 and glutamate receptor function and prevents them from counteracting amyloid-β–driven synaptic suppression.

ApoE transports cholesterol to neurons through ApoE receptors, which are members of the low-density lipoprotein (LDL) receptor gene family(11). Some of these ApoE receptors, such as LRP1, Apoer2, VLDL (very-low-density lipoprotein) receptor (Vldlr), and LRP4, are intrinsic components of central and peripheral synapses, where they serve as essential regulators of neurotransmission through cytoplasmic signaling(12, 13). The uncleaved forms of ApoE receptors mediate ApoE endocytosis and signal transduction(14). ApoE receptors can undergo sequential proteolytic cleavage much like APP and Notch(15, 16). Initial extracellular protease cleavage releases a soluble receptor fragment that antagonizes extracellular ligands(14, 17). A second intramembranous cleavage of the remaining membrane-bound C-terminal fragment of Apoer2 by γ-secretase releases an intracellular domain (ICD) into the cytoplasm (18), where it can potentially regulate transcription in a similar manner as described for LRP1(19).

Regulation of extracellular cleavage is controlled by the glycosylation state of Apoer2(18). O-linked sugars (OLSs) conjugated to the juxtamembranous OLS domain hinder access of this domain to proteases, blocking initial extracellular cleavage and preventing further processing. Reduced glycosylation of Apoer2 and LRP1 greatly increases ectodomain cleavage, implicating glycosylation as a potent post-translational regulatory mechanism of ApoE receptors(18). Both Apoer2 and Vldlr produce splice variants lacking their OLS domain(20–22). Deletion of the OLS domain of Vldlr reduces the stability of the receptor at

the membrane because of unhindered proteolytic cleavage(23). Thus, both glycosylation and differential splicing can regulate the processing and turnover of ApoE receptors.

The distribution of Apoer2 is predominantly limited to the brain, and Apoer2 is found in multiple splice variants(21, 22, 24–27). Ligand-induced Apoer2 clustering with Vldlr(28) and EphB2 receptor(29) by the secreted signaling protein Reelin mediates tyrosine phosphorylation of NR2 NMDA receptor (NMDAR) subunits, which requires a 59–amino acid insert in the Apoer2 cytoplasmic tail. Inclusion of this insert is regulated by activity that triggers alternative splicing of exon 19(30). In addition, there is a correlation between spine density and Apoer2 abundance such that spine numbers are augmented with Apoer2 overexpression and reduced in younger Apoer2 knockout (KO) neurons(31), suggesting that regulation of Apoer2 abundance can affect synapse formation.

Splicing of Apoer2 in specific exons can fine-tune ligand binding (exons 5, 7, and 9)(14, 32, 33), receptor glycosylation and processing (exon 16)(18), and downstream signaling pathways (exon 19)(30, 34). The functional consequences of these splicing events have been studied *in vitro*, but little is known about the physiological role of the extracellular OLS domain encoded by exon 16. To investigate the function of this OLS domain *in vivo*, we generated a pair of knock-in mouse strains that constitutively lack the OLS domain with and without exon 19, which we predicted would increase processing and consequently reduce Apoer2 abundance, similar to Vldlr. We found that extracellular cleavage of Apoer2 was reduced in the absence of the OLS domain. *In vivo*, OLS-deficient Apoer2 was more abundant in the brain, and consistent with the role of Apoer2 in the regulation of synapse formation, dendritic spine density and glutamate receptor abundance were also increased. Slices from mice expressing the OLS-deficient Apoer2 variant with the exon 19-encoded cytoplasmic tail had enhanced LTP, and reducing Apoer2 abundance by reducing an allele of Apoer2 to hemizygosity restored spine density and LTP to wild-type LTP values. OLS-deficient animals constitutively expressing the alternatively spliced exon 19 in the ICD showed defects in fear learning. These findings demonstrate a key role of ApoE receptors as essential regulators of synaptic glutamate receptor activity and establish differential receptor glycosylation as a regulator of synapse function.

Results

Apoer2 lacking the OLS domain is hypoglycosylated and Apoer2 protein abundance is increased *in vivo*

The OLS domain of Apoer2 is heavily glycosylated(18) and alternatively spliced in both mice and humans(21, 22, 24, 26). To probe the physiological role of differential splicing of the OLS domain, we generated two knock-in mouse lines, both of which constitutively lack the sequence encoded by exon 16. One line (Apoer2*[16+19]*) expresses exon 19, which encodes the alternatively spliced intracellular tail domain responsible for Reelin-induced increase in LTP(30), and the other line (Apoer2*[16 19]*) constitutively lacks both exons (Fig. 1A, fig. S1A). Both knock-in mouse lines were bred to homozygosity (fig. S1B) with no overt phenotypes, and neurons from these mice responded normally to Reelin, as assessed by the phosphorylation of the downstream effector Dab (fig. S2).

Glycosylation of the OLS domain protects Apoer2 from proteolytic cleavage(18). We anticipated that loss of this glycosylated region of Apoer2 would produce a hypoglycosylated Apoer2, which would be more vulnerable to extracellular proteases thus making the protein less stable and leading to decreased Apoer2 protein abundance. To determine the abundance of OLS-deficient Apoer2 in the brain, we quantified Western blots of brain membrane fractions from wild-type and Apoer2*[16]* knock-in mice probed for Apoer2 (Fig. 1B). The abundance of hypoglycosylated Apoer2 from Apoer2*[16]* knock-in brains was higher than that of properly glycosylated Apoer2 from wild-type brains. The amount of Apoer2 protein in brain membrane fractions from Apoer2*[16+19]* animals was increased two fold compared to the amount of Apoer2 in those from wild-type animals. Deletion of exon 19 (Apoer2*[16 19]*) further accentuated this Apoer2 protein increase to about three fold of wild-type values (Fig. 1B and C), suggesting that exon 19 also affects Apoer2 protein abundance. To understand whether Apoer2 protein abundance is transcriptionally or posttranscriptionally regulated, we quantified Apoer2 mRNA amounts in wild-type and Apoer2*[16]* knock-in brains (Fig. 1D). Both knock-in lines showed increased Apoer2 mRNA amounts, indicating that protein production may play a role in the increase in Apoer2 protein abundance.

To assess the glycosylation state of the OLS-deficient Apoer2 variants, we treated protein from Apoer2*[16]* knock-in and wild-type brain membrane fractions with the enzymes neuraminidase and *O*-glycosidase (Fig. 1E). The addition of sialic acid is a common modification of OLSs, and the enzyme *O*-glycosidase cannot remove glycans from amino acids where these sialic acids are present. Pretreatment with neuraminidase, which removes sialic acid from sugar chains, enables O-glycosidase to remove OLSs. Western blotting indicated that glycosidase treatments reduced the molecular weight of wild-type Apoer2 (Fig. 1E, lanes 1 to 3), but not that of Apoer2 from Apoer2*[16]* knock-in brains (Fig. 1E, lanes 4 to 9), confirming that the deleted OLS domain is required for glycosylation of Apoer2.

Glycosylation or loss of OLS domain of Apoer2 protects against proteolytic cleavage *in vitro*

Because glycosylation generally protects against proteolytic processing(35, 36), hypoglycosylation of the extracellular domain should therefore leave Apoer2 vulnerable to proteolytic cleavage and decrease the surface stability of the receptor. However, the abundance of membrane Apoer2 was significantly increased in the brains from the knock-in mice that constitutively express an OLS domain-deficient and thus hypoglycosylated form of the receptor. Because Apoer2 mRNA was also increased, we cannot rule out the possibility that *de novo* Apoer2 production may be partially responsible for the increase in protein abundance. However, it is also possible that deletion of the OLS domain not only affected normal receptor glycosylation but also disrupted or removed a protease cleavage site within the extracellular domain.

To better understand how the deletion of the OLS domain affects receptor glycosylation and cleavage, we transfected Apoer2 splice variants with exon 16 (Apoer2*[+16]*) and without exon 16 (Apoer2*[16]*) into Chinese hamster ovary (CHO-K1) cells and glycosylation-

deficient *ldlD* cells(37), which are mutant CHO-K1 cells that cannot produce some of the sugar chains required for glycosylation when maintained under galactose-free culture conditions (Fig. 2A). Thus, proteins expressed in *ldlD* cells are hypoglycosylated even when glycosylation sites are present. Lysates of transfected cells were subjected to glycosidase treatments using the enzymes neuraminidase, *O*-glycosidase, and peptide *N*-glycosidase F (PNGaseF) (Fig. 2A). Neuraminidase treatment slightly reduced the molecular weight of Apoer2*[+16]* expressed in CHO-K1 cells, which is consistent with the removal of sialic acid from the sugar chains from the receptor (Fig. 2A, lane 6). Treatment with neuraminidase and *O*-glycosidase reduced the electrophoretic mobility of the higher molecular weight band of Apoer2*[+16]* expressed in CHO-K1 cells indicating that OLSs were removed (Fig. 2A, **lane 7**). PNGaseF can remove nearly all N-linked sugar chains, and treatment with this enzyme reduced the molecular weight of both Apoer2*[+16]* bands in lysates from transfected CHO-K1 cells (Fig. 2A, lane 8). In glycosylation-deficient *ldlD* cells, Apoer2*[+16]* was hypoglycosylated as indicated by the lack of molecular weight shift after treatment with neuraminidase and *O*-glycosidase (Fig. 2A, lanes 1 to 3). However, a small shift in molecular weight remained after treatment with PNGaseF, indicating that the OLS domain could still be modified by the addition of N-acetylglucosamine sugar chains in *ldlD* cells (Fig. 2A, lane 4). On the other hand, Apoer2*[16]*, which lacks the OLS domain, was hypoglycosylated (Fig. 2A, lanes 1 to 4) irrespective of whether it was expressed in CHO-K1 cells or *ldlD* cells.

We assessed whether the OLS domain was involved in the proteolytic processing of Apoer2 by treating CHO-K1 or *ldlD* cells expressing either Apoer2*[+16]* or Apoer2*[16]* with or without the γ-secretase inhibitor DAPT to block intramembranous cleavage of the C-terminal fragment of Apoer2 by γ-secretase. Inhibition of this intramembranous cleavage should sequester the C-terminal fragment at the membrane and allow for its accumulation and detection in membrane protein fractions (Fig. 2B). Western blots of the cell lysates were probed with an antibody against the extracellular ligand-binding domain of Apoer2 or an antibody against the C-terminal tail of Apoer2 to detect the full-length and C-terminal fragment of Apoer2, respectively. We assessed the extent of proteolytic processing of Apoer2 in the transfected cells by measuring the accumulation of the C-terminal fragment in the cell lysates. The Apoer2 C-terminal fragment generated from the hypoglycosylated Apoer2*[+16]* in *ldlD* cells was increased five fold compared to the glycosylated Apoer2*[+16]* expressed in CHO-K1 cells (Fig. 2, C and D, lane 1 and 5). The C-terminal fragment produced in either cell line accumulated with DAPT treatment, confirming that this cleavage product was a γ-secretase substrate (Fig. 2C, lanes 2 and 6). Thus, when the OLS domain is present but not glycosylated, extracellular processing of Apoer2 is increased, resulting in the production of a γ-secretase substrate that can undergo further proteolytic cleavage. In cells expressing the Apoer2 mutant lacking the OLS domain, we could still detect a faint Apoer2 C-terminal fragment with some γ-secretase-dependent accumulation in either cell line.However, cells expressing Apoer2*[16]* generated significantly less C-terminal fragment than those expressing Apoer2*[+16]* (Fig. 2, C and D), indicating that the OLS domain is required for efficient and potentially site-specific proteolytic processing of Apoer2.

To further confirm the protective role of glycosylation on the cleavage of Apoer2, we generated a form of Apoer2 lacking all possible O-glycosylation sites by mutating all 29 potential serine and threonine residues in exon 16 to alanines, which cannot be glycosylated (henceforth referred to as the "alanine mutant"). We quantified the accumulation of the C-terminal fragment of Apoer2 in human embryonic kidney (HEK)–293 cells expressing the alanine mutant, Apoer2*[+16]*, or Apoer2*[16]* in the absence or presence of the γ-secretase inhibitor DAPT (Fig. 2E). Proteolytic cleavage of the alanine mutant was increased, as suggested by the reduced amount of the full-length form (3.72±1.54% of wild-type) and the increased accumulation of C-terminal fragments upon γ-secretase inhibition, compared to the Apoer2*[16]* form. The amount of C-terminal fragments was roughly comparable to the amount of full-length wild-type form recognized by the same antibody, suggesting that similar amounts of wild-type and mutant protein were produced, and that the loss of the full-length form in the mutant was most likely the result of increased proteolytic processing within the OLS-deficient juxtamembrane segment, resulting in increased turnover. This result suggests that the OLSs protect Apoer2 from extracellular cleavage and subsequent intramembranous processing.

Together, these data confirm that the OLS domain is necessary for glycosylation of the extracellular domain of Apoer2. We further conclude that the OLS domain is required for regulated proteolytic processing of Apoer2 and that *in vitro* this cleavage is controlled by glycosylation of the extracellular domain.

Loss of the OLS domain prevents extracellular metalloprotease cleavage and subsequent processing of Apoer2

Loss of the OLS domain by alternative splicing appeared to prevent the proteolytic processing of Apoer2, which results in decreased C-terminal fragment production *in vitro* (Fig.2, C and D) and increased receptor abundance *in vivo* (Fig. 1, B and C). The first step in the proteolytic processing of Apoer2 is metalloprotease-initiated cleavage of an extracellular domain (Fig. 2B), likely the OLS domain. To test how loss of the OLS domain affects the ectodomain shedding of Apoer2, we quantified extracellular proteolytic cleavage fragments in the cell media and intracellular proteolytic cleavage fragments in lysates of HEK293 cells expressing Apoer2*[+16]* and Apoer2*[16]*. As expected, soluble Apoer2 was detected in cell media collected from the Apoer2*[+16]* transfected cells, but not from the Apoer2*[16]* transfected cells (Fig. 2F, lanes 1 and 2) indicating that the OLS domain was required for specific ectodomain cleavage. Cotransfection of the metalloprotease ADAM10 (a disintegrin and metalloprotease domain-containing protein 10) augmented the amount of soluble Apoer2 released into the cell media by cells expressing Apoer2*[+16]*, but not Apoer2*[16]* (Fig. 2F, lanes 5 and 6). In Apoer2*[+16]* transfected cells, which generate the soluble form of Apoer2, the Apoer2 C-terminal fragment accumulated with DAPT-mediated inhibition of γ-secretase (Fig. 2F, lanes 3 and 7). Consistent with the loss of extracellular cleavage in Apoer2*[16]*, cells transfected with this mutant did not produce a clear singular C-terminal fragment band, rather multiple bands of varying molecular weights and slightly enhanced abundance upon γ-secretase inhibition (Fig. 2F: lanes 2,4,6,8).

These data suggest that Apoer2 proteolytic processing – a two-step process requiring extracellular cleavage mediated by matrix metalloproteases followed by intramembrane cleavage by γ-secretase resulting in the release of the Apoer2 ICD into the cytoplasm (Fig. 2D) - is similar to that of APP(15, 16) and in transfected cells requires the OLS domain.

To assess the role of the OLS domain in Apoer2 cleavage in neurons, we treated primary cortical and hippocampal neuron cultures from wild-type, Apoer2*[KO]*, Apoer2*[16]* KI mice with DAPT to measure the γ-secretase-dependent degradation of the C-terminal fragment of Apoer2. Western blotting of wild-type neurons revealed a DAPT-dependent increase in two bands, ~19 kDa and ~15 kDa, corresponding to the C-terminal fragment with and without the alternatively-spliced exon 19, respectively (Fig. 2G: lanes 1,2). As expected, immunoblots of neurons from Apoer2 null mice did not show bands that were reactive with the Apoer2 antibody (Fig. 2G: lane 3,4). Lysates from Apoer2*[16+19]* and Apoer2*[16 19]* neurons (Fig. 2G: lanes 5–8) generated fragments in the 15–25 kDa range, which were slightly enhanced by γ-secretase inhibition (Fig. 2G: lanes 6,8 to 5,7). The heterogeneous bands in Apoer2 KI neurons are likely a result of proteolytic processing of the receptor at various secondary and non-specific locations within the extracellular portion of the receptor in the absence of the domain encoded by exon 16. The lack of the specific Apoer2 C-terminal fragment found in wild-type neurons suggests that Apoer2 variants lacking exon 16 are not cleaved and the extracellular OLS domain of Apoer2 is required for specific proteolytic processing of Apoer2 in primary neuron cultures.

Increased Apoer2 stability enhances LTP in an exon 19-dependent fashion

Apoer2 can modulate synaptic plasticity mediated by the Reelin signaling pathway(38) in an exon 19-dependent manner(30). To explore the effect of increased OLS-deficient Apoer2 on synaptic plasticity, we measured long-term potentiation (LTP) of the well-characterized CA1-CA3 synapses in the hippocampus after theta burst stimulation (TBS). CA3 Schaffer collateral axons synapse onto CA1 stratum radiatum dendritic spines, and stimulation of these CA3 fibers evokes synaptic current flow which is measured extracellularly as field excitatory postsynaptic potentials (fEPSPs) in CA1 stratum radiatum (Fig. 3A). The steeper the slope of these potentials, the stronger the synapses. The potentiation of fEPSPs after TBS was significantly greater in slices from Apoer2*[16+19]* mice than in slices from wild-type mice, which had similar TBS-induced LTP as slices from Apoer2[16 19] mice (Fig. 3B). The presence or absence of the intracellular domain encoded by exon 19 of Apoer2 has previously been shown to have no effect on basal LTP induction (30). Thus, the increased LTP in Apoer2*[16+19]* slices but not the Apoer2*[16 19]* slices indicates that the enhanced LTP in Apoer2*[16+19]* slices is not solely dependent on the presence of exon 19 but requires the holoreceptor lacking the OLS domain.

We next sought to determine whether the increased Apoer2 abundance in mice expressing OLS-deficient form of the receptor (Fig. 1B,C) was responsible for the enhanced LTP in these mice (Fig. 3C,D). By crossing Apoer2*[16+19]* mice with Apoer2 KO mice, we produced Apoer2*[KO/ 16+19]* mice with similar amounts of the Apoer2*[16+19]* splice variant as total Apoer2 in wild-type mice (Fig. 3C, inset). Reducing the Apoer2*[16+19]* receptor abundance to wild-type amounts also reduced TBS-induced LTP in Apoer2*[KO/*

16+19] slices to that seen in wild-type slices (Fig. 3C,D) indicating that the regulation of Apoer2 abundance by the OLS domain can fine-tune synaptic plasticity in synergy with the exon 19-encoded tail insert.

To understand the connectivity of the potentiated CA3-CA1 synapses, we examined the relationship (as assessed by input-output curves) of the postsynaptic CA1 fEPSP slopes (output) and the amplitude of the fiber volley (input) which represents the magnitude of the CA3 Schaffer collateral presynaptic input. We found that with strong afferent input, CA1 synapses from the OLS-deficient slices were weaker than those from wild-type slices (Fig. 3E). As the presynaptic input increased, the output of postsynaptic CA1 synapses was significantly reduced in slices from Apoer2*[16+19]* mice and was further attenuated in slices from Apoer2*[16 19]* mice compared to wild-type mice (Fig. 3E), suggesting this deficit may be induced in part by exon 19. The input-output relationship of CA3-CA1 synapses in slices from Apoer2*[KO/ 16+19]* mice was statistically similar to those from wild-type mice (Fig. 3E). Together, these results indicate that augmented OLS-deficient Apoer2 expression inhibits the strength of the CA3-CA1 synapse, and that the presence of the cytoplasmic, exon 19-encoded, insert can exacerbate this effect.

When synapses are stimulated, Ca^{2+} enters the presynaptic terminal and subsequent stimulation before this initial Ca^{2+} influx can be cleared from the terminal increases the probability of synaptic vesicle release, resulting in increased presynaptic input and enhanced postsynaptic response (an effect called facilitation) (39). To determine whether presynaptic synaptic vesicle release probability was altered in the Apoer2*[16]* KI mice, we measured presynaptic facilitation (PPF) by giving two stimuli at intervals ranging from 20–200 ms and comparing the slope of the second fEPSP to the initial slope (Fig. 3G). The PPF at each interval in slices from the Apoer2*[16]* KI mice were similar to those of wild-type with the exception of reduced facilitation at the shorter, 20-ms interval in slices from Apoer2*[16+19]* mice indicating a presynaptic deficit at this stimulation frequency. This effect was not observed in the slices from Apoer2*[KO/ 16+19]* mice, suggesting that the effect is due to increased Apoer2*[16+19]*abundance (Fig. 3F).

Enhanced hippocampal LTP does not enhance spatial memory and augmented Apoer2 abundance reduces fear acquisition in an exon 19-dependent manner

Slices from Apoer2*[16+19]* animals showed abnormal synaptic transmission and LTP induction in the hippocampus, an area of the brain that is involved in both spatial and contextual learning and memory. To determine if enhanced hippocampal LTP in slices from Apoer2*[16+19]* animals conferred enhanced ability to learn, we examined hippocampal-dependent spatial memory acquisition with the Morris water maze (40). Mice were trained to reach a hidden, submerged platform in a water-filled pool over an 11-day period, and there were no significant difference in the time (Fig. 4A) and or distance traveled (Fig. 4B) before the platform was reached between the genotypes. On day 12, the submerged platform was removed and there were no significant differences between genotypes in either the time spent (Fig. 4C) or distance traveled (Fig. 4D) in the quadrant of the submerged platform.

We next tested cued and contextual fear conditioning, a paradigm that probes for hippocampal-dependent (context) and amygdala-dependent (context and cued) fear learning

((*41, 42*)). On day one, we trained each mouse to associate a sound with a foot-shock by acclimating the mouse to a novel environment and repeatedly pairing a tone with a brief foot-shock. On day two, the mice were placed back into the same environment and assessed for freezing over five minutes to measure the contextual association with the foot-shocks. On day three, the mice were placed in another novel environment for six minutes and assessed for freezing during the last three minutes when the same tone was played to measure the association of the tone with the foot-shock.

Compared to wild-type mice, the Apoer2*[16+19]* mice displayed significantly less freezing behavior during training (Fig. 4E). However, when returned to the same context the next day, the time that Apoer2*[16+19]* mice spent frozen was not statistically different from that of wild-type mice (Fig. 4F), indicating that mice of both genotypes associated the foot-shock with the context. In contrast, Apoer2*[16+19]* mice showed a reduced freezing response and Apoer2*[16 19]* mice an enhanced freezing response. When presented with the tone on day three, the Apoer2*[16+19]* mice spent almost no time freezing despite their normal hearing (Fig. S3) indicating a significant deficit in cued fear conditioning compared to wild-type mice (Fig. 4G). Reducing the abundance of Apoer2*[16+19]* to wild-type amounts rescued these deficits (Fig. 4E–G). By contrast, mice expressing the Apoer2*[16 19]* splice variant were not significantly different from wild-type mice in their ability to associate the shock with the context (Fig. 4F) or auditory cue (Fig. 4G), and displayed a significant increase in freezing in the last minute of the cue test compared to wild-type mice (Fig. 4G). These results indicate that these different splice variants of Apoer2 may play a role in the consolidation and amplitude of fear acquisition.

Alternative splicing of the OLS domain alters hippocampal spine density and glutamate receptor abundance in Apoer2*[16]* knock-in mice

Because Apoer2 overexpression stimulates synapse formation *in vitro*(31), we hypothesized that the increased Apoer2 protein abundance in Apoer2*[16]* knock-in brains would increase spine number. We quantified the spine density in Golgi-impregnated hippocampal CA1 pyramidal neurons from the brains of wild-type, Apoer2*[16+19]*, Apoer2*[16 19]* and Apoer2*[KO/ 16+19]* mice. Because spine density varies with distance from the *soma*(43), we calculated the spine density at a distance of ~115–120 μm from the base of the apical dendrite, which corresponds to the area from which fEPSPs were recorded. Compared to wild-type neurons, the average spine density was significantly increased in Apoer2*[16 19]* neurons, but not in Apoer2*[16+19]* neurons. (Fig. 5D). Apoer2*[KO/ 16+19]* and wild-type neurons had similar spine densities (Fig. 5A–D). The average cumulative distribution of spine density revealed that the range of spine densities was significantly increased in both Apoer2*[16+19]* and Apoer2*[16 19]* neurons (Fig. 5E). The correlation of spine density with Apoer2 abundance (Fig. 5F) suggests that synapse number can be regulated by alternative splicing of exon 16, through effects of Apoer2 abundance.

We next probed the composition of these synapses to further clarify the mechanism by which LTP is enhanced in Apoer2*[16+19]* but not Apoer2*[16 19]* mice (Fig. 5G,H). Quantification of total AMPA receptor protein abundance in the hippocampus indicated that

the abundance of GluA1 and GluA2/3 AMPA receptor subunits was significantly increased in Apoer2*[16 19]* mice but not in Apoer2*[16+19]* mice compared to wild-type AMPAR abundance (Fig. 5G). Similarly, the abundance of both NMDA receptor subunits, GluN2A and GluN2B, were significantly increased in the hippocampus of Apoer2*[16 19]* mice, and only GluN2B was significantly increased in the Apoer2*[16+19]* mice compared to wild-type mice (Fig. 5H).

Discussion

In this study, we present two findings regarding the role of the alternatively spliced exon 16 of Apoer2. First, this alternatively spliced OLS domain is required not only for glycosylation but also for the initial extracellular cleavage that precedes intramembranous γ-secretase-mediated release of the Apoer2 ICD. Second, loss of Apoer2 proteolytic processing results in altered synaptic formation and function *in vivo*. The absence of the OLS domain of Apoer2 leads to increased Apoer2 abundance, dendritic spine densities and glutamate receptor abundance and decreased synaptic efficacy. Physiologically, the increased Apoer2 translates into enhanced LTP in mice expressing a form of the receptor with exon 19. The augmented LTP and spine densities are reversed by reducing Apoer2 protein abundance to wild-type amounts by removing one allele of the receptor. These structural changes of synapse morphology did not translate into altered behavior or learning. The augmented hippocampal synaptic plasticity did not enhance performance in either of two hippocampal memory tasks: spatial or contextual fear learning. Intriguingly, the amygdala-dependent cued fear response was attenuated in mice expressing the OLS-deficient Apoer2 with exon 19, a deficit that required enhanced Apoer2 abundance. This observation points toward a previously unrecognized role for Apoer2 in the regulation of fear-processing circuits. Taken together, we conclude that the OLS domain is required for Apoer2 proteolytic processing, and that alternative splicing of this glycosylated extracellular domain regulates Apoer2 abundance, which alters synaptic function.

Our finding that the loss of the OLS domain prevented Apoer2 proteolytic cleavage was unexpected. Apoer2 is sequentially processed in a manner similar to APP, Notch, and its relative LRP1(15, 16, 44). Metalloproteases such as ADAM10(45, 46) cleave the extracellular domain of Apoer2 leaving a substrate for γ-secretase, which then releases the Apoer2 ICD through intramembranous cleavage(17, 18) (Fig. 2B). Although deletion of the OLS domain significantly decreased the processing of the receptor, some non-specific processing was still evident in both transfected cells and primary neuron cultures (Fig. 2). Whether these nonspecific products are physiologically functional remains to be determined.

The ability to control Apoer2 proteolytic cleavage through both alternative splicing of exon 16 and glycosylation of the encoded OLS domain suggests an important functional role for such redundant regulation. *In vivo*, loss of Apoer2 proteolytic processing resulted in increased Apoer2 abundance. While Apoer2 might be expected to be more stable because of decreased extracellular cleavage, we found a concomitant increase in Apoer2 mRNA indicating that loss of the Apoer2 ICD might also affect the transcriptional regulation of the receptor. Misexpression of one form of the receptor may render some cellular functions inoperable and the increase in Apoer2 mRNA and protein may indicate cellular

compensation to correct for improper receptor isoform abundance. To add another layer of complexity, the Apoer2 ICD contains a putative nuclear localization signal (**R**NW**KRK**NTK (47, 48)), and can localize to the nucleus and affect transcription (49), so the increased abundance of Apoer2 protein and mRNA in Apoer2*[16]* knock-in mice could indicate transcriptional control mediated by the Apoer2 ICD itself, provided the fragment has transcription regulation capabilities akin to LRP1(19).

Loss of normal Apoer2 processing in mouse lines expressing an OLS-deficient Apoer2 resulted in greater Apoer2 protein abundance and increased spine density in the apical dendrites of CA1 hippocampal neurons of both Apoer2*[16]* knock-in mice (Fig. 4). These data are consistent with previous results in which spine density is decreased in Apoer2 knockout mice and increased in neurons overexpressing Apoer2 in culture(31). Spine density is reduced in mice expressing human ApoE4(50), likely because these mice have less surface Apoer2 due to a defect in Apoer2 recycling(10). In contrast, mice expressing the human ApoE2, which is considered a protective factor against the development of Alzheimer's disease (51), show increased Apoer2 recycling and spine density(10, 50). Together, these results demonstrate that regulation of Apoer2 through alternative splicing of the OLS domain can regulate synapse formation.

While spine density was increased, overall synaptic efficacy in the same neurons was decreased. Mice expressing either Apoer2 splice variants lacking the OLS domain had reduced synaptic responses to the same presynaptic input (Fig. 3E), suggesting that alternative splicing of the OLS domain of Apoer2 can modify synaptic homeostasis. Weaker synaptic transmission coupled with augmented synapse number could be explained by a few scenarios. First, the postsynaptic efficacy of each *[16]* synapse or population of synapses could be less than those with wild-type Apoer2 because of decreased abundance, decreased conductance of postsynaptic glutamate receptors, or a combination of both. However, the abundance of both AMPA- and NMDA-type glutamate receptors was increased in the Apoer2*[16]* mutants, a finding that cannot account for the overall decrease in synaptic efficacy. A larger population of silent synapses is another possible explanation for decreased synaptic output from neurons with more synapses (52). Silent synapses contain NMDAR and no AMPAR, rendering them unresponsive to glutamate at the resting membrane potential, and can be unsilenced by the insertion of AMPAR into the postsynaptic membrane. Further biochemical and electrophysiological dissection is necessary to identify the scenario that contributes to the loss of synaptic efficacy in Apoer2*[16]* mice.

Despite the deficit in baseline neurotransmission, hippocampal slices from mice lacking exon 16 showed an exon 19-dependent increase in LTP compared to those from wild-type mice, which was lost when the abundance of the mutant Apoer2 protein was reduced to approximately wild-type amounts (Fig 3C,D). These results suggest that exon 19 plays a role in the enhanced synaptic plasticity as slices from Apoer2*[16 19]* mice did not have greater LTP than those from wild-type mice. We have previously shown that Reelin signaling leads to phosphorylation of NMDAR subunits and enhances LTP in an Apoer2 exon 19-dependent manner(30). It is possible that Apoer2*[16+19]* mice are more sensitive to endogenous Reelin due to the increased abundance of exon 19 expressing Apoer2 and therefore could show augmented NMDAR phosphorylation and increased LTP induction. Another

possibility is that exon 19 might be required for unsilencing these synapses, thus enhancing LTP in Apoer2*[16+19]* and not Apoer2*[16 19]* mice.

The alternatively-spliced cytoplasmic insert of Apoer2 (encoded by exon 19) specifically binds PSD95, JIPs and Mint1(×11α)(53, 54). PSD95 promotes activation of NMDARs as well as Apoer2 surface abundance and proteolytic cleavage (55)..The JIPs interact with JNK, which has been implicated in neuronal survival (30, 34, 54, 55). In conjunction with PSD95 and Mint1, Apoer2 can enhance or reduce dendritic spine formation and maturation(31). It may be through these adaptor or scaffolding proteins that exon 19 fine-tunes spine number and the complexity of the postsynaptic density, and could account for the differences in synaptic efficacy and LTP in the Apoer2*[16+19]* mice compared to the Apoer2*[16 19]* mice.

Apoer2 can tightly regulate its own proteolytic processing. Glycosylation of the OLS domain protects Apoer2 from cleavage, and without the OLS domain, Apoer2 processing is reduced. These endogenous OLS-deficient Apoer2 splice variants impact Apoer2 abundance, synapse number and efficacy in knock-in mice. Thus, alternative splicing and differential glycosylation of the OLS domain of Apoer2 synergistically and antagonistically regulate receptor function and highlights a mechanism to control synaptic homeostasis.

Materials and Methods

Apoer2 and ADAM10 Expression Plasmids

The Apoer2 (mouse) expression plasmid was modified from the Apoer2 full-length vector that was previously described (30) by the deletion of exon 16. The HA tagged ADAM10 vector was a gift from Dr. Stefan Lichtenthaler(56).

Antibodies

Apoer2 antibodies: tail-specific (C-terminal antibody, rabbit polyclonal affinity purified, 1:500), and extracellular antibody (against the ligand binding domain, rabbit polyclonal serum, 1:1000). Commercial antibodies: Tuj-1 monoclonal (1:10,000, Millipore), β-actin monoclonal (1:2,000, Abcam), HA-specific polyclonal for detection of ADAM10 expression (1:2000, Sigma). Glutamate receptor antibodies: GluA1 (1:1000, rabbit polyclonal, Abcam), GluA2/3 (1:2000, rabbit polyclonal, Abcam), GluN2A (1:500, Cell Signaling), GluN2B (1:1000, Cell Signaling).

Animals

All mice were housed under a 12:12 light:dark cycle and fed a normal chow diet. All animals were euthanized by inhalation of isoflurane followed by decapitation according to strict regulations set by the National Institutes of Health Guide for the Care and Use of Laboratory Animals and the UT Southwestern Animal Care and Use Committee.

Wild-type SV129 and C56BL/6J mixed background line were obtained and maintained from breeding of chimeric Apoer2*[16±19]* mice. The Apoer2 null mouse line has been previously described (30, 57). Apoer2*[±19]* knockin animals(30) were modified to create the Apoer2*[16±19]* targeting vectors. Briefly, exon 16 and surrounding intronic sequences

(1971 bps total) were deleted from the targeting vectors by using the endogenous BamHI and PmeI restriction sites. The ends were filled with the Klenow enzyme and blunt-end ligated. Targeting vectors were linearized using SalI and electroporated into mouse 129/SvJ embryonic stem cells (SM-1). G418-resistant colonies were screened by PCR and confirmed by Southern blot and sequencing analysis for homologous recombination (1% recombination efficiency). Recombined ES cells were microinjected into C57BL/6J blastocysts and resulting male chimeras were mated with female C57BL/6J mice to achieve germ-line transmission of the knockin Apoer2 allele. PCR genotyping of the Apoer2[16] lines utilized the common primer IM305 (5'-CTTCCCTGAGACACCTGTACAGCACTAG-3'), WT primer IM379 (5'-AATTCAGTGTCACATGTGTTAGGAC-3'), and knockin primer IM380 (5'-TTCCTATTCCGAAGTTCCTATTCTC-3'), yielding a 380 bp WT band and a 600 bp knockin band.

Cell lysate and membrane protein glycosidase treatment

Brain membrane fractions (20 μg) or transfected cell lysates (10 μg) were incubated (overnight, 37°C) with neuraminidase (New England Biolabs), O-glycosidase (Roche) or PNGaseF (New England Biolabs) according to manufacturer protocols. Reactions were then directly used for Western blotting by adding SDS sample buffer and running on an 8% SDS-PAGE gel. Brain membrane proteins were probed with an Apoer2 tail-specific antibody.

Brain Membrane Fraction Preparation

Whole brain was homogenized using a polytron tissue grinder in 1 ml of Buffer I (in mM: 20 Tris-HCl pH 8.0, 120 NaCl, 1 $CaCl_2$, and EDTA-free protease inhibitor cocktail) per mg of tissue. Homogenate was spun down (800 rpm, rotor JS-5.2, Beckman J-6B centrifuge, 5 min, 4°C). Supernatant was spun again (10,000g, 10 min, 4°C), and the supernatant of this spin was ultracentrifuged (55,000 rpm, TLA110 rotor, Beckman Optima TLX, 30 min, 4°C). The resulting pellet was resuspended in Buffer II (in mM: 50 Tris-HCl pH 8.0, 80 NaCl, 2 $CaCl_2$, with 1% Triton X-100, 0.1% SDS and EDTA-free protease inhibitor cocktail), homogenized by forcing the suspension 15–20 times through a 23-gauge needle, incubating on ice (10 min) and spinning again (55,000 rpm, 30 min, 4°C). The resulting supernatant contained the membrane-enriched fraction. 30 μg of the membrane protein fraction was run on 8% SDS-PAGE gels and western blotted for Apoer2.

RT-PCR

Brain tissue was homogenized in 4 ml RNA STAT-60 (1 ml/1 mg tissue, TEL-TEST, Inc.) using a polytron and incubated for 5 minutes at room temperature. 800 μl of chloroform were added to the homogenate, the sample was shaken vigorously (15 s), incubated at RT (3 min) and spun down (5,200 rpm, rotor JS-5.2, Beckman J-6B centrifuge, 30 min, 4°C). The aqueous phase was removed, added to 2 ml of isopropanol and incubated at RT (10 min) before centrifuging (20,000g, 20 min, 4°C) to precipitate RNA. The pellet was washed with ethanol and dissolved in RNase-free water. DNA was digested from the RNA sample using the DNA-free™ Kit (Applied Biosystems). cDNA was prepared using the TaqMan Reverse Transcription Reagents Kit (Applied Biosystems). Real-Time PCR reactions were set up in triplicate using SYBR Green PCR Master Mix (Applied Biosystems). The real time PCR

reaction used primers in exon 18 (which is not alternatively spliced and should account for all Apoer2 splice variants): mApoER2ex18-2F (5'-GGTAATAGCCCTGCTATGTATGAGTG-3') and mApoER2ex18-71R (5'-GCTCTTGGTGTTCTTCCGCTT-3'). The resulting Apoer2 CT values were normalized to cyclophilin CT values using the Delta-Delta CT method.

Cell line transfection and Apoer2-cleavage assessment

HEK 293 cells were cultured in DMEM (Sigma) supplemented with 10% FCS at 37°C and 8.8% CO_2. CHO-K1 cells were cultured in DMEM/F-12 (50:50, Cellgro) with 5% FCS (8.8% CO_2, 37°C). *ldlD* cells were cultured in Hams F-12 media with 5% FCS (1% pen/strep, 5% CO_2, 37°C). All cells were plated with 300,000 cells/dish and transfected with FuGENE (Roche) at 2 days *in vitro* (DIV). DAPT treatments performed 24 hours post-transfection, Cells were switched to 0% FCS media (1 hour before and during DAPT treatment). Cells were treated for 24 hours with DAPT (Sigma; 10 μM final from 20 mM stock in DMSO) or DMSO (Sigma) only for all controls before collecting culture media (containing soluble Apoer2) and cells. Cells were washed ice-cold PBS (twice) and scraped from the dish into 1ml of PBS. Cells were spun down (10,000g, 3 min, 4°C) and lysed in 5-cell volumes of 1% TritonX-100 lysis buffer (in mM: 50 Tris pH 7.4, 150 NaCl, 1 $MgCl_2$, 1 $CaCl_2$, with 1% Triton X-100 and EDTA-free protease inhibitor cocktail (Complete, mini, protease Inhibitor Cocktail Tablets, Roche)). Lysate was cleared of cell debris (20,000g, 15 min, 4°C) and used in Western blots probed with the specified antibodies.

Primary neuron cultures

Primary cortical/hippocampal neuron cultures were prepared from embryonic day 16 mouse embryos (5 brains/culture) as previously described (58). For the proteolytic processing assay, DAPT (10 μM) was added to 7 DIV culture media and incubated 24 hours. For Reelin signaling assay, conditioned media from stably transfected cells expressing Reelin or mock conditioned media was added to media of 5 DIV cultures for 30 minutes. Cells were washed twice (ice-cold PBS), collected in 1 ml of PBS, spun down and lysed in 50 μl of 1% TritonX-100 lysis buffer (in mM: 50 Tris pH 7.4, 150 NaCl, 1 $MgCl_2$, 1 $CaCl_2$, with 1% Triton X-100 and EDTA-free protease inhibitor cocktail). Protein concentrations were measured using the Lowry method and 30 μg of protein were analyzed by western blot (4–15% gradient gel, Apoer2 tail-specific antibody).

Multisite-directed mutagenesis of mouse Apoer2 exon 16

All 29 serine and threonine residues encoded by exon 16 in full-length Apoer2 (described in (30)) were converted to alanine residues using the QuikChange Multi Site-Directed Mutagenesis Kit (Agilent Technologies) and the mutagenic primers listed in Supplemental Table 1. The mutant plasmid was verified by sequencing.

Western Blot Quantification

Proteins were run on the specified SDS-PAGE gels and transferred to a nitrocellulose membrane and probed with the specified antibodies. All blots were visualized using the LI-

COR system. The integrated intensity was determined for each protein band and normalized to the loading control (β-actin or Tuj-1).

Extracellular Field Recordings

Hippocampal slices were prepared from 2–4-month-old mice. The brain was quickly removed and placed in an ice-cold high-sucrose slicing solution (in mM: 110 sucrose, 60 NaCl, 3 KCl, 1.25 NaH_2PO_4, 28 $NaHCO_3$, 0.5 $CaCl_2$, 5 glucose, 0.6 ascorbic acid, 7 $MgSO_4$). Transverse 400-μm sections were cut using a vibratome. Slices were kept in an incubation chamber containing a 1:1 ratio of artificial cerebrospinal fluid (ACSF; in mM: 124 NaCl, 3 KCl, 1.25 NaH_2PO_4, 26 $NaHCO_3$, 10 D-glucose, 2 $CaCl_2$, 1 $MgSO_4$) and slicing solution before each experiment. Slices were then transferred into an interface recording chamber kept at 31°C and superfused with ACSF (2–3 ml/min). For stimulation, concentric bipolar electrodes (FHC, CBBRC75) were placed into the stratum radiatum. Stimulus intensity was set at 40–60% of the maximum peak amplitude field excitatory postsynaptic potential (fEPSP) (calculated before firing starts) and delivered through an Isolated Pulse Stimulator (A-M Systems, Model 2100). Labview 7.0 was used to record and analyze LTP experiments. A theta burst paradigm (TBS; train of 4 pulses at 100 Hz repeated 10 times with 200 ms intervals; repeated 5 times at 10 s intervals) was used as the conditioning stimulus. Paired pulse facilitation was obtained by delivering two stimuli at 20, 50, 100, and 200 ms intervals and calculating the ratio of second fEPSP slope to the first fEPSP slope.

Animal Behavior

A Morris Water Maze station was set up with a 4-ft diameter circular aluminum pool filled with water (23°C) dyed with white, non-toxic, liquid tempera paint to make the water opaque. A plexiglass escape platform (circular, 10-cm diameter) was submerged in one of the quadrants of the pool (1-cm below the level of the water). Various prominent visual cues were placed around the pool. 3–5-month-old mice were subjected to four trials per day for 11 days. During each trial the mouse was placed into the pool in one of four starting locations (North, South, East, or West) and allowed to find the submerged platform. Once the mouse found the platform it was left there for 10 seconds before being removed and placed back into the holding cage. If the mouse did not find the platform within 60 seconds it was then guided to the platform and again left for 10 seconds before being removed. On days 5 and 9 the first of the four trials was a probe test (the mouse was allowed to free swim for 60 seconds with the submerged platform removed). On day 12 only the probe test was performed. Mouse movements were tracked by video camera and the HSVimage software. Latency to reach the platform and distance traveled to reach the platform were analyzed for each mouse during the 11-day training period. Percent time spent and distance traveled in the goal quadrant, where the submerged platform used to be, was analyzed for each of the three probe tests. The experimenter was blind to the genotype of the animals.

To assess fear conditioning, mice were placed in a shock chamber (Med Associates Inc., St. Albans, VT) on day one for a 6-minute training period, during the last three minutes of which they were exposed to three parings (1-min interval) of a 20-s tone immediately followed by a 2-s, 0.5mA foot-shock. On day two, mice were placed in the training context

for 5 minutes and the level of freezing was recorded. On day three, mice were placed in a different context for 6 minutes, and during the last 3 minutes the tone was played. Mouse freezing was recorded with the FreezeFrame program and analyzed using the FreezeView program. Normal nociception of all animal strains was ascertained by registering comparable locomotor and vocal responses to the shock application.

To assess acoustic startle responses, mice were placed in a test chamber (SR-Lab Systems, San Diego Instruments) with background noise (70 dB) for 5 minutes and a series of thirteen 40-ms acoustic tones of were played randomly (70–118 dB, in 4-dB increments, 10–20s intervals). This series was repeated four times for each mouse. The startle response was quantified as the maximum startle from 65 ms after the onset of the acoustic tone.

Golgi-impregnation of neurons

The FD Rapid GolgiStain™ Kit (FD NeuroTechnologies, PK401) was used to impregnate neurons according to the kit manual. In brief, after isofluorane anesthesia and decapitation, brains from 8–12-week-old mice were rapidly removed and rinsed with ACSF and placed into 2.5–3 ml of a 1:1 mixture of solution A and B, which was premixed 24 hours previous. The mixture was replaced the next day and brains were incubated at room temperature for 3 weeks in the dark. After 3 weeks, the mixture of solution A and B was removed and replaced with solution C and stored at 4°C. The next day, the solution C was refreshed and brains were incubated at 4°C for 1 to 4 weeks. Horizontal sections (150–200 μm thick) were cut with a Leica VT1200 in an ice-cold 6% sucrose solution. Slices were rinsed in solution C and placed on a gelatinized slide (2%) coated with a thin layer of solution C (3–4 sections per slide). After the whole brain was sectioned, excess moisture was removed from the slides and slices were pressed into the gelatin by placing parafilm over the slices and applying gentle downward pressure without moving the slices side to side. The slides were either immediately processed according to the kit's instructions or kept in a slightly humid chamber for up to 3 days before processing and sealed with Permount® (Fisher) and a coverslip (no.1 thickness).

Slides containing the central CA1 region of the hippocampus without genotype indicators and 5–8 neurons were analyzed for each animal (at least 3 animals per genotype, for a total of 14–25 neurons per genotype). Bright field images of CA1 neurons were obtained using a Zeiss Axioplan2 microscope, AxioCam MR camera, and AxioVision 4.7 and proper Kohler illumination (0.9 air condenser). For each neuron, a 20X image stack (2 μm z-interval) of the entire neuron and 63X image stack (0.6 μm z-interval) of the apical dendrite was obtained. Images shown in Figure 5C are an extended focus of high magnification image stacks containing the region of interest (ROI) with the Extended Depth of Field plugin(59) for Fiji (NIH).

To calculate spine density, a distance of 115 μm was measured from the start of the apical dendrite at the soma with Fiji (NIH) and a region of dendrite (average length ~25 μm) was selected and spines were manually counted by scrolling through the image stack and selecting spines with the Point Tool and automatic addition to the ROI manager tool. All ROI selections were saved and the length of dendrite, number of spines, and distance from the soma were recorded. The spine density (spines/μm) was calculated for each neuron by

dividing the number of spines counted by the length of dendrite (in μm). The average values reported for each genotype were calculated by averaging the values for each animal (5–8 neurons each) and then averaging those values for each genotype. Individual cumulative distributions of spine density were calculated per animal and averaged for each genotype to calculate the reported average cumulative distribution.

Glutamate Receptor Protein Quantification

Hippocampi were dissected from 8-week-old male mice and homogenized with ice-cold RIPA lysis buffer (in mM: 50 Tris-HCl pH 8.0, 150 NaCl, 2 $MgCl_2$, 2 EDTA and 1% NP-40) by forcing the suspension 15–20 times through a 23-gauge needle. Homogenates were spun down (14,000 rpm, 15 min, 4°C) before assessing the protein concentration with the Bio-Rad D_c protein assay. SDS sample buffer was added to 10 μg of protein and incubated (5 min, 100°C) before running on a 4–15% SDS-PAGE gel (Bio-Rad).

Statistical Analysis

Statistical analyses were performed with Graphpad Prism 6 software using one of the following tests: Student's t-test, one-way and two-way ANOVA with Tukey's *post hoc* multiple comparisons test for exact multiplicity adjusted p-values between groups. When using one-way ANOVA, all data sets were checked for normality with the D'Agostino & Pearson omnibus or KS normality test. If data was non-normal, the non-parametric Kruskal-Wallis test was performed with Dunn's *post hoc* multiple comparisons test.

Supplementary Material

Refer to Web version on PubMed Central for supplementary material.

Acknowledgments

References and Notes

1. Glenner GG, Wong CW. Alzheimer's disease: initial report of the purification and characterization of a novel cerebrovascular amyloid protein. Biochemical and biophysical research communications. 1984; 120:885–890. [PubMed: 6375662]

2. Masters CL, Simms G, Weinman NA, Multhaup G, McDonald BL, Beyreuther K. Amyloid plaque core protein in Alzheimer disease and Down syndrome. Proceedings of the National Academy of Sciences of the United States of America. 1985; 82:4245–4249. [PubMed: 3159021]

3. Kang J, Lemaire HG, Unterbeck A, Salbaum JM, Masters CL, Grzeschik KH, Multhaup G, Beyreuther K, Muller-Hill B. The precursor of Alzheimer's disease amyloid A4 protein resembles a cell-surface receptor. Nature. 1987; 325:733–736. [PubMed: 2881207]

4. Chen QS, Kagan BL, Hirakura Y, Xie CW. Impairment of hippocampal long-term potentiation by Alzheimer amyloid beta-peptides. Journal of neuroscience research. 2000; 60:65–72. [PubMed: 10723069]

5. Selkoe DJ. Alzheimer's disease is a synaptic failure. Science. 2002; 298:789–791. [PubMed: 12399581]

6. Shankar GM, Li S, Mehta TH, Garcia-Munoz A, Shepardson NE, Smith I, Brett FM, Farrell MA, Rowan MJ, Lemere CA, Regan CM, Walsh DM, Sabatini BL, Selkoe DJ. Amyloid-beta protein dimers isolated directly from Alzheimer's brains impair synaptic plasticity and memory. Nature medicine. 2008; 14:837–842.

7. Durakoglugil MS, Chen Y, White CL, Kavalali ET, Herz J. Reelin signaling antagonizes beta-amyloid at the synapse. Proceedings of the National Academy of Sciences of the United States of America. 2009; 106:15938–15943. [PubMed: 19805234]

8. Rebeck GW, Reiter JS, Strickland DK, Hyman BT. Apolipoprotein E in sporadic Alzheimer's disease: allelic variation and receptor interactions. Neuron. 1993; 11:575–580. [PubMed: 8398148]

9. Strittmatter WJ, Roses AD. Apolipoprotein E and Alzheimer's disease. Annual review of neuroscience. 1996; 19:53–77.

10. Chen Y, Durakoglugil MS, Xian X, Herz J. ApoE4 reduces glutamate receptor function and synaptic plasticity by selectively impairing ApoE receptor recycling. Proceedings of the National Academy of Sciences of the United States of America. 2010; 107:12011–12016. [PubMed: 20547867]

11. Herz J, Bock HH. Lipoprotein receptors in the nervous system. Annual review of biochemistry. 2002; 71:405–434.

12. Herz J, Chen Y. Reelin, lipoprotein receptors and synaptic plasticity. Nat Rev Neurosci. 2006; 7:850–859. [PubMed: 17053810]

13. Dieckmann M, Dietrich MF, Herz J. Lipoprotein receptors--an evolutionarily ancient multifunctional receptor family. Biological chemistry. 2010; 391:1341–1363. [PubMed: 20868222]

14. Koch S, Strasser V, Hauser C, Fasching D, Brandes C, Bajari TM, Schneider WJ, Nimpf J. A secreted soluble form of ApoE receptor 2 acts as a dominant-negative receptor and inhibits Reelin signaling. The EMBO journal. 2002; 21:5996–6004. [PubMed: 12426372]

15. Shah S, Lee SF, Tabuchi K, Hao YH, Yu C, LaPlant Q, Ball H, Dann CE 3rd, Sudhof T, Yu G. Nicastrin functions as a gamma-secretase-substrate receptor. Cell. 2005; 122:435–447. [PubMed: 16096062]

16. Zheng H, Koo EH. The amyloid precursor protein: beyond amyloid. Molecular neurodegeneration. 2006; 1:5. [PubMed: 16930452]

17. Hoe HS, Rebeck GW. Regulation of ApoE receptor proteolysis by ligand binding. Brain Res Mol Brain Res. 2005; 137:31–39. [PubMed: 15950758]

18. May P, Bock HH, Nimpf J, Herz J. Differential glycosylation regulates processing of lipoprotein receptors by gamma-secretase. J Biol Chem. 2003; 278:37386–37392. [PubMed: 12871934]

19. Zurhove K, Nakajima C, Herz J, Bock HH, May P. Gamma-secretase limits the inflammatory response through the processing of LRP1. Science signaling. 2008; 1 ra15.

20. Sakai J, Hoshino A, Takahashi S, Miura Y, Ishii H, Suzuki H, Kawarabayasi Y, Yamamoto T. Structure, chromosome location, and expression of the human very low density lipoprotein receptor gene. J Biol Chem. 1994; 269:2173–2182. [PubMed: 8294473]

21. Clatworthy A, Stockinger W, Christie R, Schneider W, Nimpf J, Hyman B, Rebeck G. Expression and alternate splicing of apolipoprotein E receptor 2 in brain. Neuroscience. 1999; 90:903–911. [PubMed: 10218790]

22. Sun XM, Soutar AK. Expression in vitro of alternatively spliced variants of the messenger RNA for human apolipoprotein E receptor-2 identified in human tissues by ribonuclease protection assays. European journal of biochemistry / FEBS. 1999; 262:230–239. [PubMed: 10231386]

23. Magrane J, Casaroli-Marano RP, Reina M, Gafvels M, Vilaro S. The role of O-linked sugars in determining the very low density lipoprotein receptor stability or release from the cell. FEBS letters. 1999; 451:56–62. [PubMed: 10356983]

24. Kim DH, Iijima H, Goto K, Sakai J, Ishii H, Kim HJ, Suzuki H, Kondo H, Saeki S, Yamamoto T. Human apolipoprotein E receptor 2. A novel lipoprotein receptor of the low density lipoprotein receptor family predominantly expressed in brain. J Biol Chem. 1996; 271:8373–8380. [PubMed: 8626535]

25. Kim DH, Magoori K, Inoue TR, Mao CC, Kim HJ, Suzuki H, Fujita T, Endo Y, Saeki S, Yamamoto TT. Exon/intron organization, chromosome localization, alternative splicing, and

transcription units of the human apolipoprotein E receptor 2 gene. J Biol Chem. 1997; 272:8498–8504. [PubMed: 9079678]

26. Brandes C, Novak S, Stockinger W, Herz J, Schneider WJ, Nimpf J. Avian and murine LR8B and human apolipoprotein E receptor 2: differentially spliced products from corresponding genes. Genomics. 1997; 42:185–191. [PubMed: 9192837]

27. Korschineck I, Ziegler S, Breuss J, Lang I, Lorenz M, Kaun C, Ambros PF, Binder BR. Identification of a novel exon in apolipoprotein E receptor 2 leading to alternatively spliced mRNAs found in cells of the vascular wall but not in neuronal tissue. J Biol Chem. 2001; 276:13192–13197. [PubMed: 11152697]

28. Strasser V, Fasching D, Hauser C, Mayer H, Bock HH, Hiesberger T, Herz J, Weeber EJ, Sweatt JD, Pramatarova A, Howell B, Schneider WJ, Nimpf J. Receptor clustering is involved in Reelin signaling. Mol Cell Biol. 2004; 24:1378–1386. [PubMed: 14729980]

29. Bouche E, Romero-Ortega MI, Henkemeyer M, Catchpole T, Leemhuis J, Frotscher M, May P, Herz J, Bock HH. Reelin induces EphB activation. Cell research. 2013; 23:473–490. [PubMed: 23318582]

30. Beffert U, Weeber EJ, Durudas A, Qiu S, Masiulis I, Sweatt JD, Li WP, Adelmann G, Frotscher M, Hammer RE, Herz J. Modulation of synaptic plasticity and memory by Reelin involves differential splicing of the lipoprotein receptor Apoer2. Neuron. 2005; 47:567–579. [PubMed: 16102539]

31. Dumanis SB, Cha HJ, Song JM, Trotter JH, Spitzer M, Lee JY, Weeber EJ, Turner RS, Pak DT, Rebeck GW, Hoe HS. ApoE receptor 2 regulates synapse and dendritic spine formation. PloS one. 2011; 6:e17203. [PubMed: 21347244]

32. Hibi T, Mizutani M, Baba A, Hattori M. Splicing variations in the ligand-binding domain of ApoER2 results in functional differences in the binding properties to Reelin. Neuroscience research. 2009; 63:251–258. [PubMed: 19167437]

33. Brandes C, Kahr L, Stockinger W, Hiesberger T, Schneider WJ, Nimpf J. Alternative splicing in the ligand binding domain of mouse ApoE receptor-2 produces receptor variants binding reelin but not alpha 2-macroglobulin. J Biol Chem. 2001; 276:22160–22169. [PubMed: 11294845]

34. Beffert U, Nematollah Farsian F, Masiulis I, Hammer RE, Yoon SO, Giehl KM, Herz J. ApoE receptor 2 controls neuronal survival in the adult brain. Curr Biol. 2006; 16:2446–2452. [PubMed: 17174920]

35. Van den Steen P, Rudd PM, Dwek RA, Opdenakker G. Concepts and principles of O-linked glycosylation. Critical reviews in biochemistry and molecular biology. 1998; 33:151–208. [PubMed: 9673446]

36. Schjoldager KT, Clausen H. Site-specific protein O-glycosylation modulates proprotein processing - deciphering specific functions of the large polypeptide GalNAc-transferase gene family. Biochimica et biophysica acta. 2012; 1820:2079–2094. [PubMed: 23022508]

37. Kingsley DM, Kozarsky KF, Hobbie L, Krieger M. Reversible defects in O-linked glycosylation and LDL receptor expression in a UDP-Gal/UDP-GalNAc 4-epimerase deficient mutant. Cell. 1986; 44:749–759. [PubMed: 3948246]

38. Weeber E, Beffert U, Jones C, Christian J, Forster E, Sweatt J, Herz J. Reelin and ApoE receptors cooperate to enhance hippocampal synaptic plasticity and learning. J Biol Chem. 2002; 277:39944–39952. [PubMed: 12167620]

39. Zucker RS, Regehr WG. Short-term synaptic plasticity. Annual review of physiology. 2002; 64:355–405.

40. Morris RG, Garrud P, Rawlins JN, O'Keefe J. Place navigation impaired in rats with hippocampal lesions. Nature. 1982; 297:681–683. [PubMed: 7088155]

41. Schafe GE, Nader K, Blair HT, LeDoux JE. Memory consolidation of Pavlovian fear conditioning: a cellular and molecular perspective. Trends in neurosciences. 2001; 24:540–546. [PubMed: 11506888]

42. Phillips RG, LeDoux JE. Differential contribution of amygdala and hippocampus to cued and contextual fear conditioning. Behavioral neuroscience. 1992; 106:274–285. [PubMed: 1590953]

43. Konur S, Rabinowitz D, Fenstermaker VL, Yuste R. Systematic regulation of spine sizes and densities in pyramidal neurons. Journal of neurobiology. 2003; 56:95–112. [PubMed: 12838576]

44. May P, Reddy YK, Herz J. Proteolytic processing of low density lipoprotein receptor-related protein mediates regulated release of its intracellular domain. J Biol Chem. 2002; 277:18736–18743. [PubMed: 11907044]

45. Hoe HS, Wessner D, Beffert U, Becker AG, Matsuoka Y, Rebeck GW. F-spondin interaction with the apolipoprotein E receptor ApoEr2 affects processing of amyloid precursor protein. Mol Cell Biol. 2005; 25:9259–9268. [PubMed: 16227578]

46. Hoe HS, Cooper MJ, Burns MP, Lewis PA, van der Brug M, Chakraborty G, Cartagena CM, Pak DT, Cookson MR, Rebeck GW. The metalloprotease inhibitor TIMP-3 regulates amyloid precursor protein and apolipoprotein E receptor proteolysis. J Neurosci. 2007; 27:10895–10905. [PubMed: 17913923]

47. Kalderon D, Roberts BL, Richardson WD, Smith AE. A short amino acid sequence able to specify nuclear location. Cell. 1984; 39:499–509. [PubMed: 6096007]

48. Kosugi S, Hasebe M, Matsumura N, Takashima H, Miyamoto-Sato E, Tomita M, Yanagawa H. Six classes of nuclear localization signals specific to different binding grooves of importin alpha. J Biol Chem. 2009; 284:478–485. [PubMed: 19001369]

49. Balmaceda V, Cuchillo-Ibanez I, Pujadas L, Garcia-Ayllon MS, Saura CA, Nimpf J, Soriano E, Saez-Valero J. ApoER2 processing by presenilin-1 modulates reelin expression. FASEB journal : official publication of the Federation of American Societies for Experimental Biology. 2013

50. Dumanis SB, Tesoriero JA, Babus LW, Nguyen MT, Trotter JH, Ladu MJ, Weeber EJ, Turner RS, Xu B, Rebeck GW, Hoe HS. ApoE4 decreases spine density and dendritic complexity in cortical neurons in vivo. J Neurosci. 2009; 29:15317–15322. [PubMed: 19955384]

51. West HL, Rebeck GW, Hyman BT. Frequency of the apolipoprotein E epsilon 2 allele is diminished in sporadic Alzheimer disease. Neuroscience letters. 1994; 175:46–48. [PubMed: 7970208]

52. Malenka RC, Nicoll RA. Silent synapses speak up. Neuron. 1997; 19:473–476. [PubMed: 9331339]

53. Minami SS, Sung YM, Dumanis SB, Chi SH, Burns MP, Ann EJ, Suzuki T, Turner RS, Park HS, Pak DT, Rebeck GW, Hoe HS. The cytoplasmic adaptor protein X11alpha and extracellular matrix protein Reelin regulate ApoE receptor 2 trafficking and cell movement. FASEB journal : official publication of the Federation of American Societies for Experimental Biology. 2010; 24:58–69. [PubMed: 19720620]

54. Gotthardt M, Trommsdorff M, Nevitt MF, Shelton J, Richardson JA, Stockinger W, Nimpf J, Herz J. Interactions of the low density lipoprotein receptor gene family with cytosolic adaptor and scaffold proteins suggest diverse biological functions in cellular communication and signal transduction. J Biol Chem. 2000; 275:25616–25624. [PubMed: 10827173]

55. Hoe HS, Pocivavsek A, Chakraborty G, Fu Z, Vicini S, Ehlers MD, Rebeck GW. Apolipoprotein E receptor 2 interactions with the N-methyl-D-aspartate receptor. J Biol Chem. 2006; 281:3425–3431. [PubMed: 16332682]

56. Lichtenthaler SF, Dominguez DI, Westmeyer GG, Reiss K, Haass C, Saftig P, De Strooper B, Seed B. The cell adhesion protein P-selectin glycoprotein ligand-1 is a substrate for the aspartyl protease BACE1. J Biol Chem. 2003; 278:48713–48719. [PubMed: 14507929]

57. Trommsdorff M, Gotthardt M, Hiesberger T, Shelton J, Stockinger W, Nimpf J, Hammer R, Richardson J, Herz J. Reeler/Disabled-like disruption of neuronal migration in knockout mice lacking the VLDL receptor and ApoE receptor 2. Cell. 1999; 97:689–701. [PubMed: 10380922]

58. Bock HH, Jossin Y, May P, Bergner O, Herz J. Apolipoprotein E receptors are required for reelin-induced proteasomal degradation of the neuronal adaptor protein Disabled-1. J Biol Chem. 2004; 279:33471–33479. [PubMed: 15175346]

59. Forster B, Van De Ville D, Berent J, Sage D, Unser M. Complex wavelets for extended depth-of-field: a new method for the fusion of multichannel microscopy images. Microscopy research and technique. 2004; 65:33–42. [PubMed: 15570586]
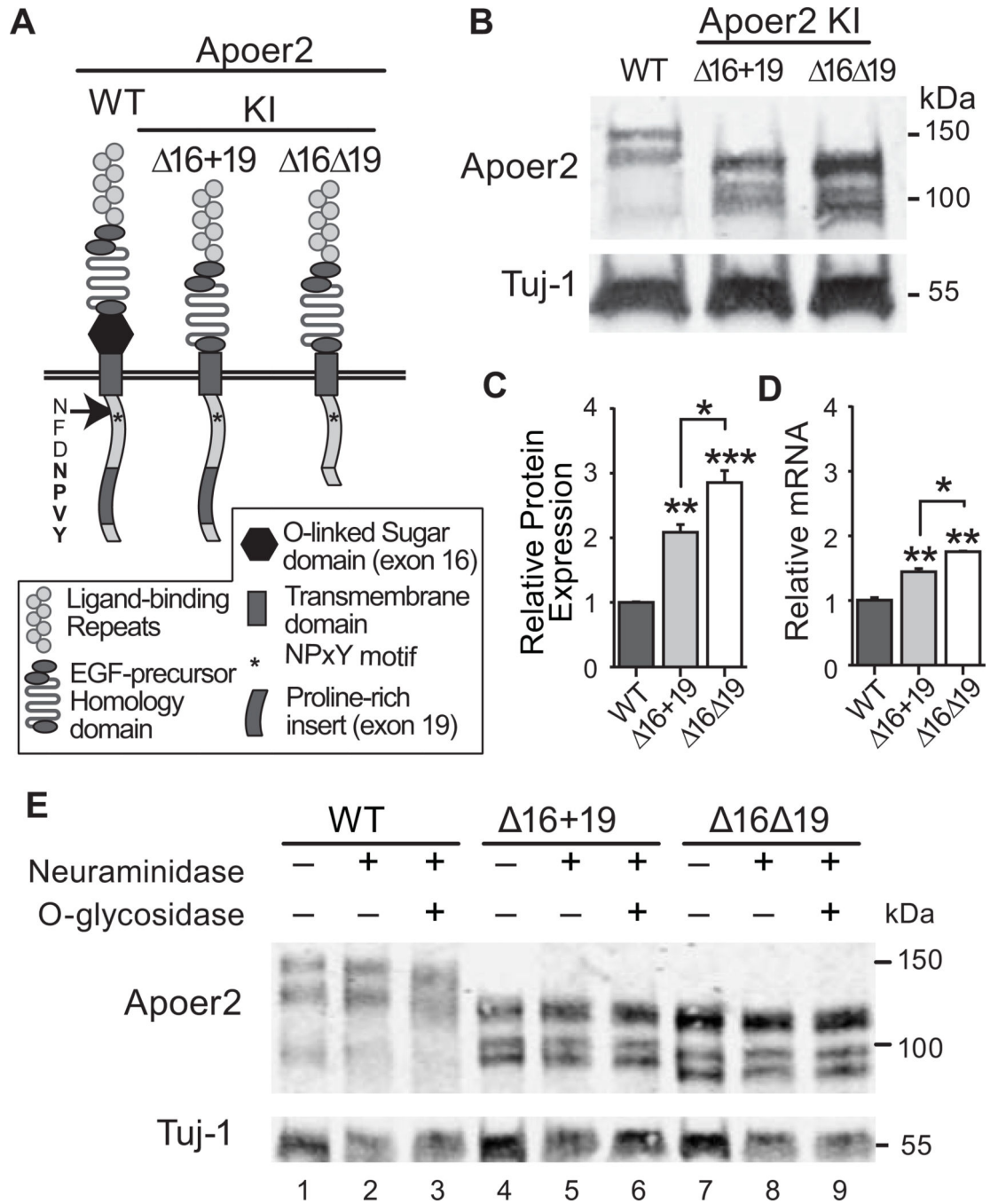
Fig. 1. Increased Apoer2 protein and mRNA abundance in Apoer2 [16] knockin mutant mouse lines

(**A**) Diagram of the protein domains of Apoer2*[16+19]* and Apoer2*[16 19]*. Apoer2*[FL]* is the wild-type (WT) full-length Apoer2 receptor included for comparison. (**B-C**) Apoer2 protein abundance in brain membrane fractions of Apoer2 knockin mice. (**B**) Representative immunoblot of Apoer2 in brain membrane fractions from WT, Apoer2*[16+19]* and Apoer2*[16 19]* mice. (**C**) Summary plot of the average Apoer2 intensity normalized to tubulin (Tuj-1) in (**B**) (mean ± sem, n= 6 mice per genotype, one-way ANOVA,

$F_{(2,15)}$=41.27, p< 0.0001; Tukey's *post-hoc:* *p= 0.0012, **p=0.0009, ***p<0.0001). (**D**) Summary plot of the mean relative quantification of Apoer2 mRNA from qRT-PCR analysis from WT, Apoer2*[16+19]* and Apoer2*[16 19]* mouse brains (mean ± sem, n= 4–6 animals per genotype, one-way ANOVA, $F_{(2,7)}$=39.95, p<0.0001; Tukey's *post-hoc:* *p=0.0130, **p=0.0022, ***p<0.0001). (**E**) Apoer2 immunoblot of brain membrane fractions from WT, Apoer2*[16+19]* and Apoer2*[16 19]* mice treated with both neuraminidase and O-glycosidase to remove O-linked sugars. (n=2 independent experiments).
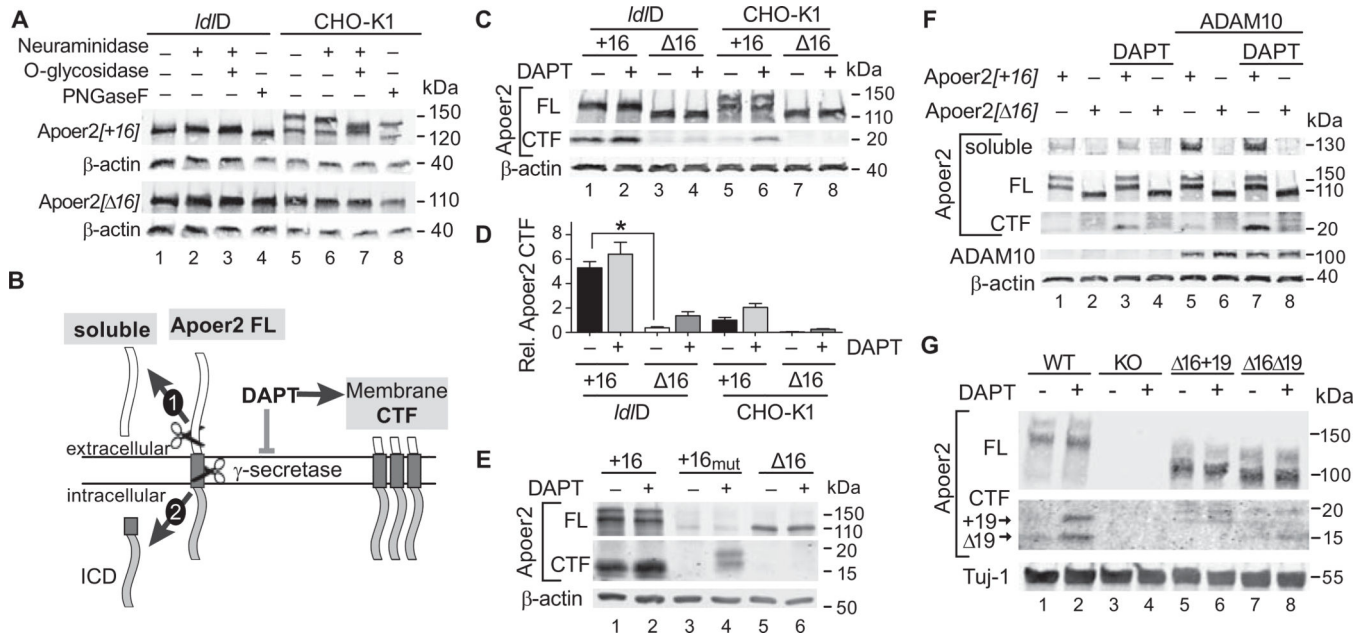
Fig. 2. Glycosylation or loss of OLS domain of Apoer2 protects against specific proteolytic cleavage by preventing extracellular metalloprotease cleavage and subsequent processing of Apoer2

(**A**) Lysates from glycosylation-deficient *ldlD* cells and wild-type CHO-K1 cells transfected with Apoer2 splice variants (Apoer2*[+16]* or Apoer2*[Δ16]*) and treated with glycosidases to remove N- and O-linked sugars (n=2 independent experiments). (**B**) Diagram of stepwise Apoer2 proteolytic processing: (i) extracellular cleavage by metalloproteases releasing the soluble extracellular domain from the CTF; (ii) intramembrane cleavage of CTF by γ-secretase releasing the intracellular ICD. DAPT treatment inhibits γ-secretase resulting in CTF accumulation. (**C-D**) Proteolytic processing of Apoer2 in glycosylation-deficient cells. (**C**) Representative immunoblot of *ldlD* and CHO-K1 cells transfected with either Apoer2*[+16]* or Apoer2*[Δ16]* with and without the γ-secretase inhibitor DAPT. (**D**) Quantification of Apoer2 CTF intensity in (**C**). (mean±sem, n=6 independent experiments, Kruskal-Wallis test, $H_{(8,48)}= 42.87$, P<0.0001, Dunn's *post-hoc*, *p= 0.0365) (**E**) Immunoblot of Apoer2-CTF accumulation in HEK-293 cells transfected with an Apoer2 plasmid lacking all potential glycosylation sites ("+16$_{mut}$") or Apoer2 constructs containing (Apoer2*[+16]*, "+16") or lacking exon 16 (Apoer2*[Δ16]*, "Δ16"). (n=6 independent experiments) (**F**) Immunoblot of Apoer2 cleavage fragments in media ("soluble") and cell lysates ("FL" and "CTF") of HEK-293 cells transfected with an Apoer2 construct containing (Apoer2*[+16]*) or lacking exon 16 (Apoer2*[Δ16]*). (n=3 independent experiments) (**G**) γ-secretase-dependent CTF-accumulation in primary neuron cultures prepared from Apoer2 KO, KI, and WT mouse lines. (n=2 independent experiments).
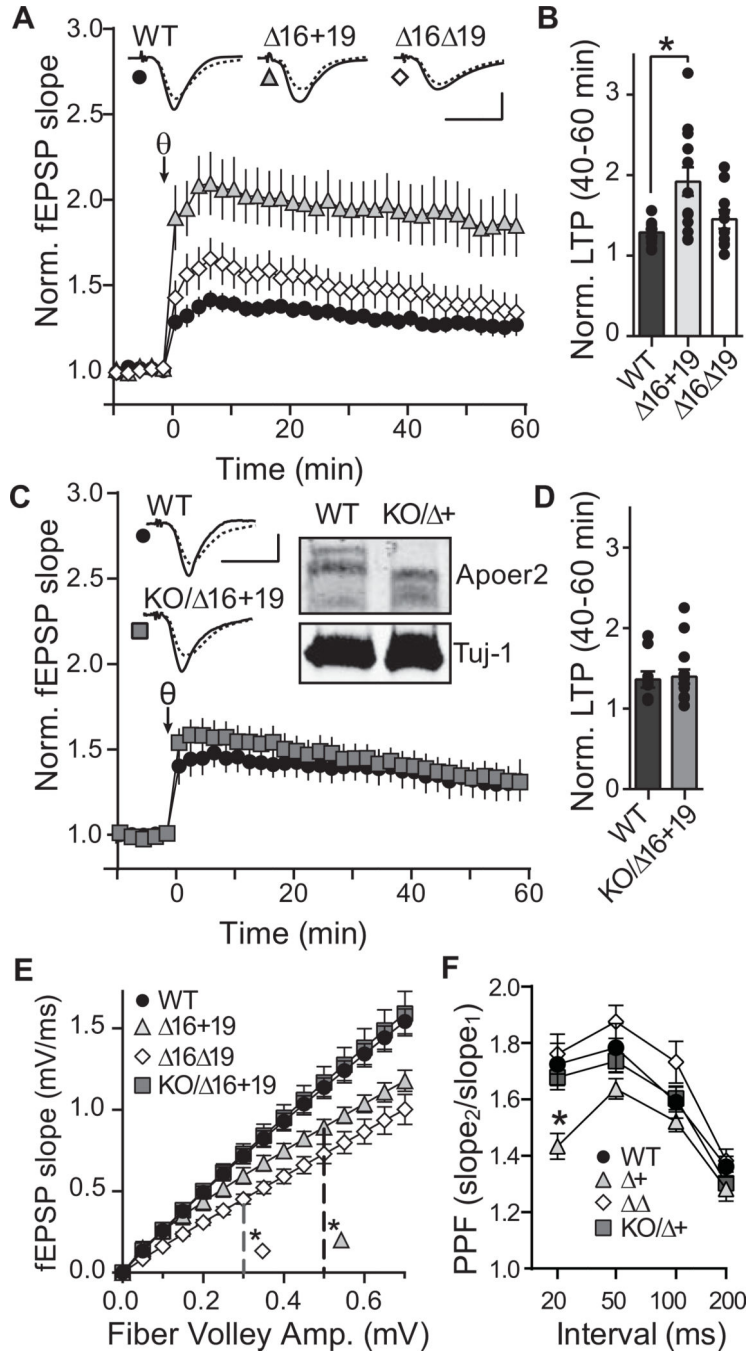
Fig. 3. OLS-deficient Apoer2 enhances LTP in an exon 19-dependent fashion
(**A to D**) Synaptic plasticity. (**A and B**) Slices from wild-type (WT) and Apoer2*[16]*
knock-in mice reveal an exon 19–dependent increase in LTP. (**A**) Summary plot of CA1
fEPSP slope before and after LTP induction by TBS (θ) of Schaffer collaterals [normalized
(norm.) to pre-TBS slope] from WT (slices = 16,animals= 3, black circles),
Apoer2*[16+19]*(slices=13, animals=5, gray triangles) and Apoer2*[16 19]*(slices=15,
animals=4, white diamonds) mice. Inset shows representative fEPSP traces 10 min before
(dashed line) and 50 min after TBS (solid line). (**B**) Average potentiation of fEPSP slope at

40–60 min after the TBS in (**A**) (one-way ANOVA, $F_{(2, 36)}$=5.294, P=0.0097; Tukey's *post-hoc*, *p=0.0126). (**C**) Average fold change in fEPSP slope before and after TBS in WT slices and slices from Apoer2*[16+19]* mice with only one Apoer2 allele (Apoer2*[KO/ 16+19]* gray square) and reduced Apoer2 protein abundance (inset; n=10 independent experiments). Summary plot of average normalized fEPSP before and after TBS in WT (slices=8, animals=4) and Apoer2*[KO/ 16+19]* (slices=15, animals=5) mice. Inset shows representative fEPSP traces 10 min before (dashed line) and 50 min after TBS (solid line). (**D**) Average fEPSP potentiation 40–60 min after the TBS in (**C**) (unpaired t-test, two-tailed: $t_{(22)}$=0.2557, p=0.8006). (**E and F**) Baseline synaptic transmission (**E**) Plot of the average fit of individual CA3 fiber volley amplitudes compared to CA1 fEPSP slope (input-output curve) before TBS recorded from WT and Apoer2 knock-in hippocampal slices (two-way RM ANOVA, simple effects within rows, genotype interaction, $F_{(3, 58)}$=6.494, P=0.0007, Tukey's *post-hoc*, *p<0.05; WT, slices=15, animals=7; Apoer2*[16+19]*, slices=15, animals=6; Apoer2*[16 19]*, slices=12, animals=5; Apoer2*[KO/ 16+19]*, slices=20, animals=6). (**F**) Average paired pulse facilitation of fEPSP slope at 20, 50, 100, and 200 ms [two-way repeated-measures ANOVA, genotype interaction, $F_{(3, 27)}$ = 3.588, P = 0.0265; Tukey's post hoc, *P = 0.0013; WT, slices = 9, animals = 3;Apoer2*[16+19]*, slices = 8, animals = 2; Apoer2*[16 19]*, slices = 8, animals = 2; Apoer2*[KO/ 16+19]*, slices = 6, animals = 2]. Error bars represent SEM. Scale bars are 2 mV and 10 ms.
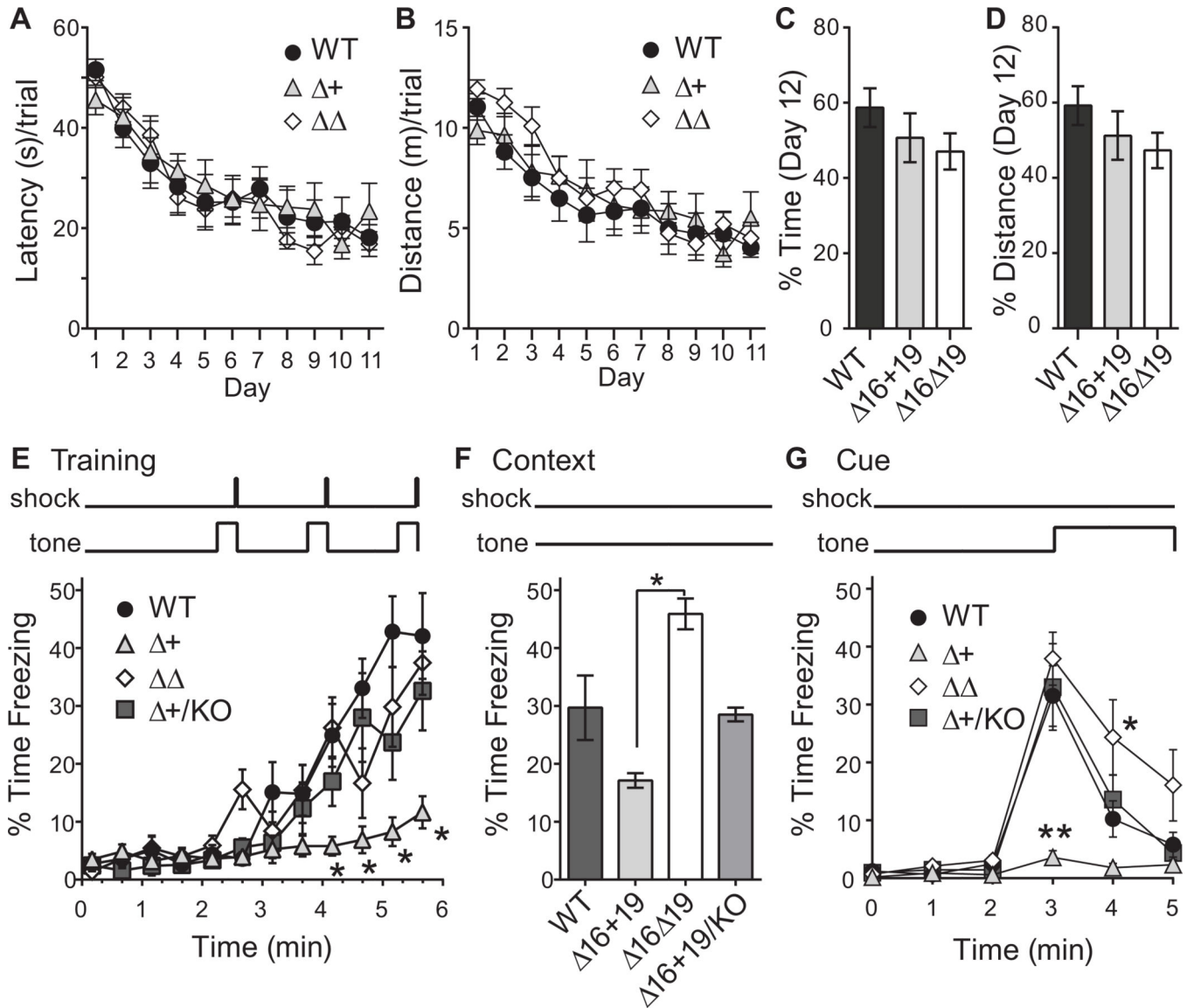
Fig. 4. Normal spatial learning and exon 19-dependent impairment fear conditioning in OLS-deficient Apoer2 mice

(**A-D**) Morris water maze (WT, n=9 mice; Apoer2*[16+19]*, n=10 mice; Apoer2*[16 19]*, n=11 mice). (**A**) Average time required to find the platform plotted in days, four trials per day for eleven days (mean ± sem; two-way RM ANOVA, genotype interaction, $F_{(2, 27)}=0.08239$, P=0.9211). (**B**) Average distance mice traveled before finding the submerged platform plotted per day (mean ± sem; two-way RM ANOVA, genotype interaction, $F_{(2, 27)}=0.4255$, P=0.6577). (**C**) Average percent time spent in the goal quadrant after training when platform was removed (mean ± sem; one-way ANOVA, $F_{(2, 27)}=1.139$, P=0.3352). (**D**) The distance traveled in the goal quadrant after training when platform was removed (mean ± sem; one-way ANOVA, $F_{(2, 27)}=1.191$, P=0.3193). (**E-G**) Cued and contextual fear conditioning (WT, n=14 mice; Apoer2*[16+19]*, n=19 mice; Apoer2*[16 19]*, n=20 mice; Apoer2*[KO/ 16+19]*, n=12 mice). (**E**) Average freezing behavior during the fear conditioning task. (mean ± sem; two-way RM ANOVA, genotype

interaction, $F_{(3, 61)}$= 4.669, P = 0.0053; Tukey's *post hoc*, *p< 0.0001). (**F**) Average freezing behavior over 5 minutes 24-h after training, in the same context in which training was carried out on day 1 (mean ± sem; one-way ANOVA $F_{(3, 61)}$=6.284, P = 0.0009; Tukey's *post hoc*, *p=0.0003). (**G**) Average freezing behavior in the same context 48-h after training; tone was played for the last 3 minutes (mean ± sem; two-way RM ANOVA, genotype interaction, $F_{(3, 61)}$=8.590, P < 0.0001; Tukey's *post hoc*, *p=0.0079, **p< 0.0001).
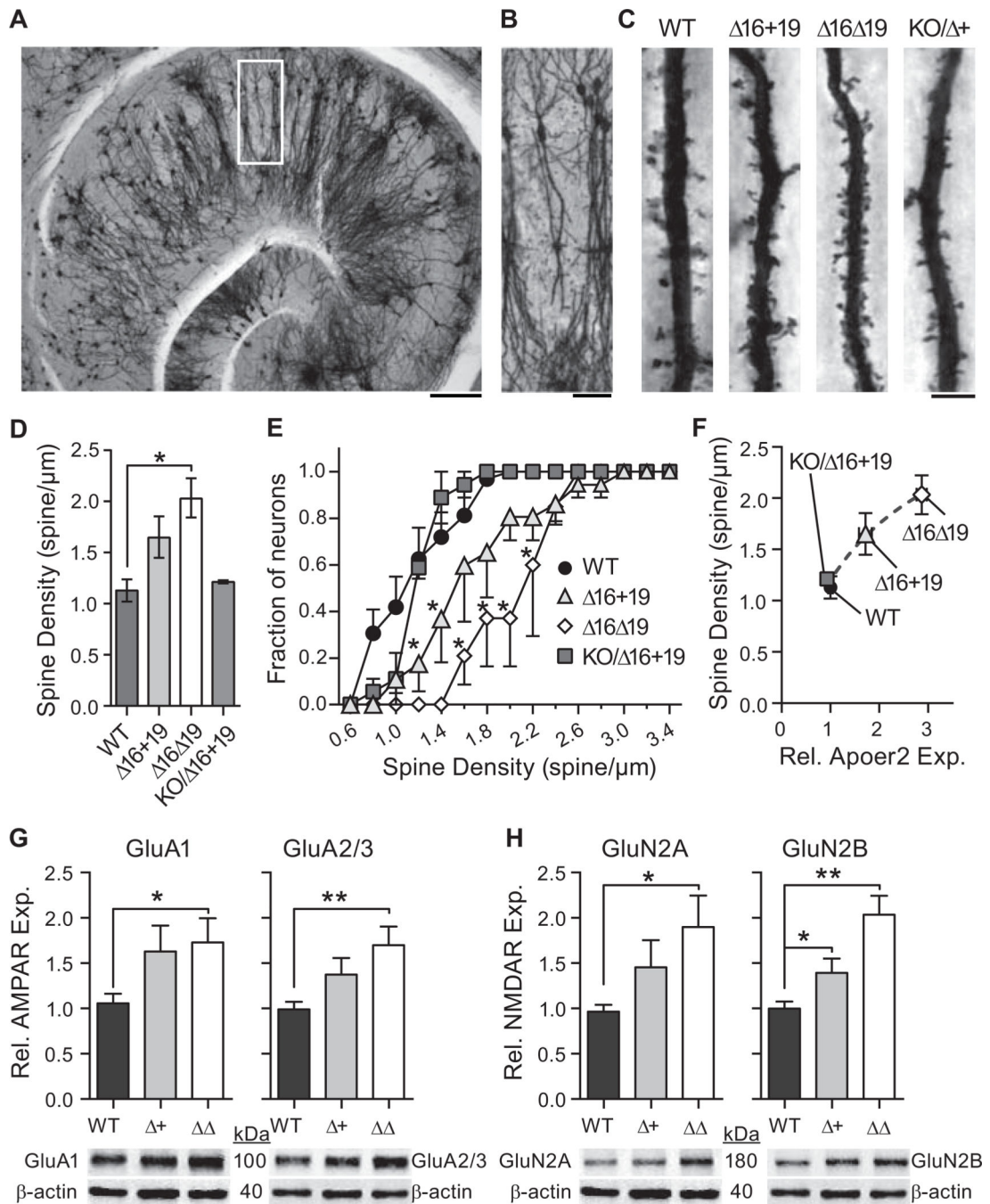
Fig. 5. Altered hippocampal CA1 spine density and glutamate receptor abundance in OLS-deficient Apoer2 mice

(**A**) Low magnification image (5X) of the hippocampus in a Golgi-impregnated slice (scale bar, 200 μm). (**B**) Higher magnification (10X) of the inset in (**A**) containing CA1 neurons (scale bar, 50 μm). (**C**) Representative images of primary CA1 apical dendrites (approximately 115 μm from the soma; scale bar, 5 μm). (**D**) Average dendritic spine density measured along dendrites of Golgi-impregnated CA1 hippocampal neurons obtained from WT (n = 25 total neurons, 4 animals), Apoer2*[16+19]* (n=19 total neurons, 3 animals),

Apoer2*[16 19]* (n=16 total neurons, 3 animals) and Apoer2*[KO/ 16+19]* (n=14 total neurons, 3 animals) mice. *[16]* knock-in mice showed an increase in spine density compared to WT (one-way ANOVA, $F_{(3, 9)}$=8.473, p=0.0055, Tukey's multiple comparisons: *p=0.006). Apoer2*[KO/ 16+19]* mice with Apoer2 protein abundance at WT amounts showed comparable spine densities as WT mice. (**E**) Summary plot depicting the average cumulative distribution of spine densities for each genotype (two-way RM ANOVA, genotype interaction, $F_{(3, 9)}$= 8.292, p=0.006, Tukey's *post-hoc:* *p 0.001). (**F**) Plot of the average Apoer2 abundance compared to the spine density for each genotype demonstrating a strong correlation of Apoer2 abundance to spine density in the absence of exon 16 (non-linear fit, one-site binding, p=0.81, $F_{(1,13)}$=0.0544). (**G–H**) Total glutamate receptor protein abundance (normalized to β-actin) in CA1 hippocampal whole-cell lysates obtained from WT, Apoer2*[16+19]* and Apoer2*[16 19]* mice (n=8 animals/genotype). Summary graphs and representative western blots showing the normalized glutamate receptor abundance: (**G**) AMPA-type (GluA1 and GluA2/3); (H) NMDA-type (GluN2A and GluN2B). (GluA1, p=0.17; GluA2/3, p=0.50; GluN2A, p=0.29; GluN2B, *p=0.047) (GluA1, *p=0.048; GluA2/3, **p=0.002; GluN2A, *p=0.041; GluN2B, **p=0.0005). Values are mean ± sem and compared by one-way ANOVA (GluA1, $F_{(2, 21)}$=3.433, p=0.0523; GluA2/3, GluA1, $F_{(2, 21)}$=8.611, p=0.0019; GluN2A, $F_{(2, 21)}$=3.471, p=0.0498; GluN2B, $F_{(2, 21)}$=10.38, p=0.0007). Tukey's *post-hoc* multiple comparisons used for individual comparisons between genotypes for each receptor.